The controlled synthesis of $Y_2O_3:Eu^{3+}$ nanotubes self-assembled into flower aggregates, nanotubes, nanospheres

ZOU Xing, LIU Pujun, YU Xibin*

(College of life and Environment Sciences, Shanghai Normal University, Shanghai 200234, China)

Abstract: Monodisperse Y_2O_3 flower aggregates were obtained by self-assembly of nanotubes through rolling up the $Y(OH)CO_3$ nanosheets without any templates under hydrothermal condition followed by an annealing process. Through decreasing the concentration of $Y(CH_3COO)_3$, homogeneous separated Y_2O_3 nanotubes with the length of(150 nm and the diameter of(40 nm and monodisperse (30 nm Y_2O_3 nanospheres were also selectively prepared. Doped Eu^{3+} ions don't influence their morphologies. Under UV excitation, $Y_2O_3:0.05Eu^{3+}$ flower-like and spherical samples show strong red emission, corresponding to the characteristic lines of Eu^{3+}.

Key words: $Y_2O_3:Eu^{3+}$; assembled; luminescent properties

CLC number: O 612.3 **Document code:** A **Article ID:** 1000-5137(2013)01-0081-09

1 Introduction

Yttrium, one of the important rare earth elements, offers applications in a broad range of fields. For example, yttrium oxide is commonly used as an excellent host material for phosphors because of the good qualities, such as broad transparency range(0.2 - 8 μm), high refractive index(>1.9), large band gap (5.8 eV), low phonon energy, and ease to be doped with rare earth ions etc[1-5]. As the main and unsurpassed red emitting materials in fluorescent lamps and flat panel devices, $Y_2O_3:Eu^{3+}$ phosphors inevitably gather more attention due to its good luminescent characteristic, acceptable atmospheric stability, reduced degradation under applied voltages, and the lack of hazardous constituents as opposed to sulfide phosphors[6-9].

The shape, size, and phase of materials with dependent properties have been well established. The synthesis of metal oxide particles with controllable shape, size, and phase is thus a key goal in materials chemistry[10-13]. Specific morphologies such as nanorods, nanowires, nanocores, nanodots, nanobundles, nanospheres, and nano? owers show great promise in many applications, as they usually exhibit electronic, optical, magnetic, and catalytic properties which are distinct as compared to their corresponding bulk

Received date: 2012-11-20

Foundation item: This work was supported by Shanghai Science and Technology Development Fund(11ZR1426500) and the Key Laboratory of Resource Chemistry of Ministry of Education of China.

Biography: ZOU Xin(1985 -), male, graduate student, College of Life and Environment Sciences, Shanghai Normal University; YU Xibin(1956 -), male, professor, College of Life and Environment Sciences, Shanghai Normal University.

* Corresponding author

materials [14-15]. Over the past decade, various morphologies of Y_2O_3: Eu^{3+} have been synthesized via different methods, including nanoparticles through combustion [16-17], microemulsion [18], and chemical vapor technique [19]; nanowires induced by template-assisted growth in AAO [20]; spherical particles by using spray pyrolysis method [21-22], urea homogeneous precipitation [23-24], and Pechini sol-gel process [25]. Remarkably, hollow nano/micro structures currently represent one of the fastest growing areas compared with other structural and geometric features [26-27]. Y_2O_3: Eu^{3+} hollow microspheres were prepared via a urea-based homogeneous precipitation technique in the presence of colloidal carbon spheres as hard templates followed by a subsequent heat treatment process [28]. One dimension(1D) Y_2O_3: Eu^{3+} nanotubes were synthesized through the template-free hydrothermal approach, following a rolling up mechanism from two dimensional(2D) nanosheets [29-30]. Recently, keen efforts have been put into using low-dimensional nanoscale materials, including nanotubes, nanorods, nanosprings, nanowires, and nanobelts as building blocks to assemble micro- and nanostructures that have highly specific morphology, novel properties and great potential applications in many fields such as photochemistry, superconductors, optoelectronics, solar cells, and catalysis [31-34].

In this manuscript, $Y(OH)CO_3$: Eu^{3+} flower aggregates assembled with nanotubes as building blocks were prepared through two steps. $Y(OH)CO_3$: Eu^{3+} nanosheets were initially prepared by a urea precipitation method and then were transferred into nanotubes assembled flower aggregates under hydrothermal conditions. $Y(OH)CO_3$: Eu^{3+} samples were decomposed into Y_2O_3: Eu^{3+} and the flower structures were maintained in the postannealing process. The influence of initial $Y(CH_3COO)_3$ concentration was systmetically investigated. Especially, the monodisperse (30 nm Y_2O_3: Eu^{3+} nanospheres were gained at extremely low initial $Y(CH_3COO)_3$ concentration. At last, the luminescent properties of Y_2O_3: Eu^{3+} of nanotube assembled flower structures and monodisperse were studied.

2 Experimental Section

Materials: All chemicals were used as received without further purification. Yttrium acetate ($Y(CH_3COO)_3 \cdot 6H_2O$) (99.99%) and Europium acetate ($Eu(CH_3COO)_3 \cdot 6H_2O$) (99.99%) were purchased from Sigma-Aldrich. PEG - 1000 and urea (A. R.) were purchased from Aladin Reagents Corporation.

Synthesis of Y_2O_3: Eu^{3+}: 6.25 mmol of $Y(CH_3COO)_3 \cdot 6H_2O$ and $Eu(CH_3COO)_3 \cdot 6H_2O$ with the Y/Eu molar ratio of 0.95/0.05 was added to 150 mL of distilled water in a 250 mL three-necked round-bottom flask. Then 3.0 g of urea and 2.5 g of PEG - 1000 were dissolved in the solution after vigorous stirring to form a clear solution. The solution was heated at 90 ℃ for 2 h with vigorous stirring before the product was collected by centrifugation. The precursors were washed by distilled water and ethanol three times. Then, the collected precursors were homogeneously re-dispersed in 35 mL of distilled water and transferred to a 50 mL autoclave with a Teflon linear at 200 ℃ for 2h. The products collected by centrifugation were dried at 60 ℃ in air. Lastly, the final products were obtained through a heat treatment at 600 or 800 ℃ in air for 2 h with a heating rate of 1 ℃ · min^{-1}.

Characterization: X-ray powder diffraction(XRD) pattern was recorded using a Japan Regaku D/max cA X - ray diffractometer equipped with graphite monochromatized Cu Kα radiation($\lambda = 1.5418$ Å) irradiated with a scanning rate of 4 deg/min. The Field-emission scanning electron microscopic (FESEM) images were obtained using a JEOL JSM - 7500F microscope operated at an acceleration voltage of 15 kV. A JEOL JEM-200CX microscope operating at 160 kV in the bright-field mode was used for Transmission Electron Microscopy (TEM). Selected area electron diffraction (SAED) pattern was performed on a JEOL JEM-2010 electron

microscope operating at 200 kV. The photo-luminescent-excitation(PLE) and photoluminscence(PL) spectra were measured by Varian spectrum meter and performed at room temperature. Elemental analyses of Y and Eu^{3+} in the solid samples were carried out on inductive coupled plasma(ICP) atomic absorption spectrometric analysis(POEMS,TJA) .

3　Results and Discussion

3.1　Formation process and phase identification

The main process in this method can be mainly divided into three steps:

(1) formation of precursor by a homogeneous precipitation method using urea as the precipitating agent (90 ℃) .

(2) morphology transition of the above obtained precursor in a hydrothermal process.

(3) formation of Y_2O_3: Eu^{3+} by calcinating the precursor in air at 600 and 800 ℃.

Step 1 is a classical precipitation method to synthesize Y(OH) CO_3, which is the idea precursor for the formation of Y_2O_3 [24] . In this step, urea serves as a reservoir for precipitation anions. The decomposition of urea releases precipitating anions, mainly OH^- and CO_3^{2-}, slowly and homogeneously into the reaction systems at elevated temperature and results in the homogeneous precipitation of the uniform Y(OH) CO_3 nano-/micro-particles [28] . In the precipitation process, the addition of surfactants and chelating agents and the coexistence of anion ions, such as Cl^-, NO_3^- and Ac^- had an important influence in controlling the morphologies of Y(OH) CO_3, such as nanospheres, nanoflkes and nanorods [35] . In our case, ultra thin nanosheets of Y(OH) CO_3 were obtained. In step 2, the nanotube-assembled flower structures of Y(OH) CO_3 were obtained via the aggregated and rolled-up nanosheets under the hydrothermal condition. In the calcinations process of step 3, the precursors decompose and transform into Y_2O_3 crystalline. All the chemical reactions can be described as follows,

$$Y^3 + (NH_2)_2CO + 3H_2O \rightarrow Y(OH)CO_3 + 2NH_4^+ + H^+ \quad (\text{step1})$$

$$Y(OH)CO_3 \rightarrow Y_2O_2 + H_2O + 2CO_2 \quad (\text{step3})$$

Figure 1 shows the XRD results of the products obtained in these three steps. No obvious diffraction peak appears in Figure 1a and Figure 1b, indicating that the yttrium compound precursors collected after precipitation and hydrothermal treatment are amorphous. This is a common phenomenon in the urea precipitation of Y(OH) CO_3. The component of precursors has be confirmed as Y(OH) CO_3 by FT-IR and TGA-DSC in many reported works, including our own previously reported work [28-35] . After the precursor was calcined at 600 ℃, all the diffraction peaks can be well indexed to the reported Y_2O_3 data in JCPDS File No. 05 - 0574, which reveals the doped Eu^{3+} ions have no influence in the Y_2O_3 phase. The high intensity of the diffraction peaks indicates good crystallinity of the nanoparticles.

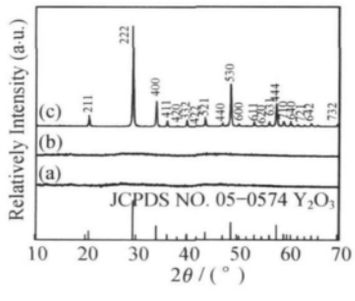

Figure 1　XRD patterns of(a) the Y(OH) CO_3: Eu^{3+} precursors after precipitation, (b) the Y(OH) CO_3: Eu^{3+} precursors after hydrothermal treatment and the Y_2O_3: Eu^{3+} sample calcined at 600 ℃

3.2 Typical morphologies of $Y(OH)CO_3:Eu^{3+}$ nanosheet precursors and nanotube-assembled flowers of $Y(OH)CO_3:Eu^{3+}$ and $Y_2O_3:Eu^{3+}$

The morphologies of the $Y(OH)CO_3:Eu^{3+}$ products collected after precipitation(step 1) and further hydrothermal treatment(step 2) are shown in figure 2. The low-magnification SEM image(Figure 2a) reveals that the $Y(OH)CO_3:Eu^{3+}$ precursors collected after precipitation are uniform in large scale. They are composed of large irregularly shaped and ultrathin nano pieces. While, after the hydrothermal treatment, great morphological changes take place in these $Y(OH)CO_3:Eu^{3+}$ precursors. The collected $Y(OH)CO_3:Eu^{3+}$ hydrothermal products consist of nanotube self-assembled flower structures with a relatively narrow size distribution(Figure 2b). A careful observation of the enlarged SEM images(Figure 2d) in several parts of this sample clearly demonstrates that the flower structures have a diameter of about 400 nm and each branch is of tube-like morphology. A number of nanotubes were found to be highly oriented, vertically aligned with high density, and extended outward from the center of each self-assembled structure. The nanotube assembled structure is further confirmed by the TEM image(Figure 2c). Each individual nanotube has an average diameter of(30 nm and a length of(200 nm. The thickness is about 8.12 nm and the inner diameter is about 6.24 nm.

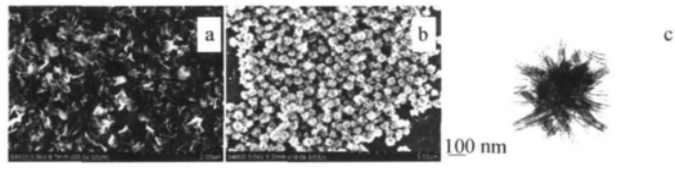

Figure 2 (a) SEM images of $Y(OH)CO_3:Eu^{3+}$ precipitated by urea at 90 ℃ for 2h; (b) SEM images and(c) TEM images of $Y(OH)CO_3:Eu^{3+}$ after the hydrothermal treatment at 200 ℃ for 2h

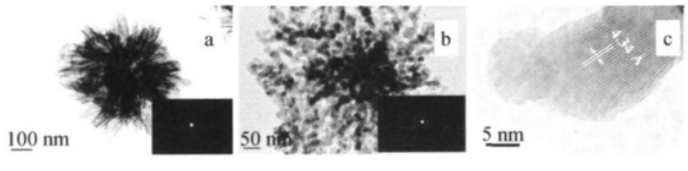

Figure 3 (a) TEM images of $Y_2O_3:Eu^{3+}$ calcined at 600 ℃, inset in(a) is the corresponding SAED pattern; (b) TEM images and(c) High resolution TEM image of $Y_2O_3:Eu^{3+}$ calcined at 800 ℃ and inset in(b) is the corresponding SAED pattern

The hydrothermal $Y(OH)CO_3:Eu^{3+}$ products decompose into $Y_2O_3:Eu^{3+}$ through calcination treatment at different temperature. Figure 3a shows a typical SEM image of 3D self-assembled $Y_2O_3:Eu^{3+}$ architectures calcined at 600 ℃. It can be seen that the calcination treatment at 600 ℃ did not cause any significant changes in shape of the product; namely, the $Y_2O_3:Eu^{3+}$ particles inherited their precursors' nanotube assembled flower morphology, whereas their size is slightly shrunk in comparison with that of the precursor in that the density of the former is higher than that of the latter. Such a transformation was common for decomposing rare earth compounds [36-37]. The SAED pattern(insert of Figure 3a) clearly shows a series of diffraction circles, indicating their characteristic polycrystalline. The $Y(OH)CO_3:Eu^{3+}$ precursors were also calcined at a higher temperature of 800 ℃. As shown in figure 3b, the TEM image shows that the 3D assembled $Y_2O_3:Eu^{3+}$ architecures are still monodisperse and remain the precursors' radial structures. But, the branched

nanotubes completely collapse, shrink and turn into conglutinated nanograins at such a high temperature. As a result, the hollow structure of nanotubes was replaced by a necklace-like structure. At the same time, high calcination temperature increases the crystalline of Y_2O_3: Eu^{3+}. The typical high resolution TEM image shows clear lattice fingers, which are not observed in the precursors and the samples calcined at low temperature. The interplanar spacing is 0.434 nm that corresponds to the (211) plane of the Y_2O_3. As shown in the SAED pattern (the insert of Figure 3b) taken from the branched nanograins, several regular diffraction lattices exist with bright concentric diffraction rings, different from the sample calcined at 600 ℃. Of course, these diffraction rings also indicate that the Y_2O_3: Eu^{3+} products with the conglutinated nanograins as building units are still polycrystalline rather than single crystalline.

3.3 The effect of the concentration of $Y(CH_3COO)_3$ on the morphology evolution of the as-prepared samples

The initial concentration of $Y(CH_3COO)_3$ in the precipitation step affects the morphology of $Y(OH)CO_3$: Eu^{3+} sample. In our above typical synthesizing process, 6.25 mmol of $Y(CH_3COO)_3$ was used in the precipitation step. Now, the PEG mass, the urea mass, the water volume and reaction temperature were kept constant (2.5 g, 3 g, 150 mL and 90 ℃, respectively), and the amount of $Y(CH_3COO)_3$ was changed from 7.8125 mmol (1.5×6.25 mmol), 4.6875 mmol (0.75×6.25 mmol) to 3.75 mmol (0.6×6.25 mmol). The precipitation and hydrothermal treatments are the same as the typical synthesizing process in the experimental section. Their morphologies are shown in figure 4, a for 7.8125 mmol, b for 4.6875 mmol and c for 3.75 mmol. The difference in their fine structures is clearly observed. When the amount of $Y(CH_3COO)_3$ is 7.8125 mmol and 4.6875 mmol, the products collected by hydrothermal treatments are nanotube self-assembled flowers. But, the amount of nanotube components decreases obviously with decreasing the $Y(CH_3COO)_3$ concentration in the precipitation process. The flower diameter also decreases from 800 nm to 300 nm. When the amount of $Y(CH_3COO)_3$ is further reduced to 3.75 mmol, the sample is composed of separated single-wall $Y(OH)CO_3$ nanotubes with the length of 150 nm. We can understand this morphology evolution from the growth mechanism. In the rolling up process, the ultrathin nanosheets and nanotubes have high chemical potential, they tend to aggregate together and form radial flower structures. When the $Y(CH_3COO)_3$ concentration decreases, the adjacent precipitated nanosheets are rather far, the rolled nanosheets have little chance to form big flower structures.

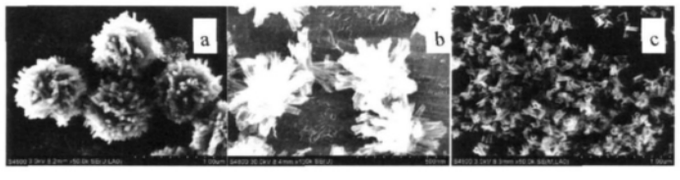

Figure 4　SEM images of the hydrothermal $Y(OH)CO_3$: Eu^{3+} products using different amount of $Y(CH_3COO)_3$, (a) 7.8125 mmol, (b) 4.6875 mmol and (c) 3.75 mmol

When the initial amount of $Y(CH_3COO)_3$ is further decreased to 3.125 mmol (0.5×6.25 mmol) and other synthesizing parameters are kept constant, great changes in the mophorlogy take place. As shown in figure 5a, they are composed of monodisperse 30 nm nanospheres in large scale, obviously different from the nanosheet products prepared at high $Y(CH_3COO)_3$ concentration. For comparison, these nanosphere products were also treated under the same hydrothermal condition. As shown in figure 5b, no morphology evolution is observed and they are still 30 nm nanospheres. The $Y(OH)CO_3$ particles prepared through urea precipitation

method normally tend to grow into spherical structures [24,35,38]. In our proposed method, adsorption of CH_3COO^- ions makes them grow towards 2D directions and form nanosheet structures. When the $Y(CH_3COO)_3$ concentration is very low, the amount of CH_3COO^- ions in the reacting system is not high enough to ensure the 2D growth. The growth behavior of $Y(OH)CO_3$ particles goes back to their natural tendency, spherical growth. The PEG works as a stabilizer, reducing agglomeration and maintaining homogeneous precipitation of $Y(OH)CO_3$ products.

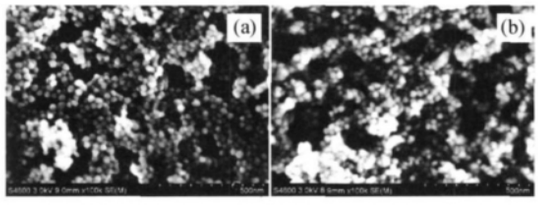

Figure 5 SEM images of $Y(OH)CO_3:Eu^{3+}$ after precipitation(a) and hydrothermal treatment(b), respectively

3.4 The luminescent properties of $Y_2O_3:Eu^{3+}$ with different shapes

In order to know the exact doping concentration of the Eu^{3+} in the samples, inductive coupled plasma (ICP) atomic absorption spectrometric analysis was used. The actual doping concentrations of Eu^{3+} in Y_2O_3 is 4.8 mol % and 4.7 mol % (Eu^{3+}/Eu^{3+} Y^{3+}) for nanotube assembled flower structures and nanospherical samples, respectively. As shown in figure 6a and b, the photoluminescence excitation (PLE) spectra of the flower-like and spherical $Y_2O_3:Eu^{3+}$ samples, monitored at 611 nm, show a strong broadband at about 244 nm and weak sharp lines in the longer wavelength region, which are due to the charge transfer band (CTB) between the O^{2-} and Eu^{3+} ions and the f-f transition of the Eu^{3+} ions, respectively. Upon excitation into the CTB of the Eu^{3+} ions at 244 nm, the emission spectrum (Figure 6 A and B) is composed of a group of lines peaking at about 552, 586, 611 and 630 nm. They come from the $^5D_1 - {}^7F_1$ and $^5D_0 - {}^7F_J$ ($J = 0, 1, 2, 3$) transitions of the Eu^{3+} ions, respectively. The presence of the emission line from higher excited states ($^5D_1$) of the Eu^{3+} ions is attributed to the low vibration frequency of Y-O bond because the multiphonon relaxation by Y-O vibration is not able to completely bridge the gap between the $^5D_1$ and $^5D_0$ levels of the Eu^{3+} ions. It is important to note that the emission intensity of the nanotube assembled $Y_2O_3:Eu^{3+}$ flowers is higher than that

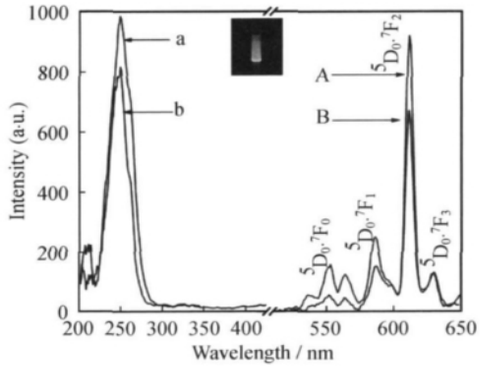

Figure 6 The PLE and PL spectra of(a, A) the nanotuble self-assembled flowers and(b, B) nanosperical $Y_2O_3:Eu^{3+}$, $\lambda_{ex} = 276$ nm, $\lambda_{em} = 611$ nm

of the nanospherical Y_2O_3: Eu^{3+}. This can be explained from the comparative low crystalline of the later sample, proved by their XRD patterns. The inset image shows the photograph of the nanotube assembled Y_2O_3: Eu^{3+} flower samples dispersed in water, irradiated by 254 nm UV emission lamp, indicating it exhibits bright red emission. As well known, Y_2O_3 is a promising host material for Er^{3+} and Dy^{3+} because Er_2O_3, Dy_2O_3 and Y_2O_3 have the same crystal structures with very similar lattice constants, and Y^{3+} and Tb^{3+} trivalent ions have similar ionic radii. Hence, it is believed that these ions doped Y_2O_3 samples with similar morphologies can also be prepared by our proposed methods and show good luminescent properties.

4　Conclusion

In summary, monodisperse nanotube self-assembled Y_2O_3 flowers and homogeneous separated Y_2O_3 nanotubes were selectively prepared on a large scale without any template through rolling up the $Y(OH)CO_3$ nanosheet under the high-temperature hydrothermal condition, following by a postcalcining treatment. The $Y(OH)CO_3$ nanosheets precusors were synthesized via precipitating $Y(CH_3COO)_3$ by urea at 90 ℃ for 2h with vigorous stirring. In this precipitation process, the existence of CH_3COO^- ions is a key factor in the formation of sheets-like structures. The concentration of $Y(CH_3COO)_3$ is another key factor in the shape-controlled synthesis. With decreasing the concentration of $Y(CH_3COO)_3$, the amount of the constituted nanotubes of flower structures and the flower size decrease. Further decreasing this concentration will lead to the formation of monodisperse Y_2O_3 nanotubes with the length of ~ 150 nm and the diameter of ~ 40 nm. At very low concentration of $Y(CH_3COO)_3$, only ~ 30 nm Y_2O_3 nanospheres were obtained. Doped Eu^{3+} ions don't influence their morphologies. Under UV excitation, Y_2O_3: 0.05Eu^{3+} flower-like and spherical samples show strong red emission, corresponding to the characteristic lines of Eu^{3+}.

References:

[1] TANNER P A, WONG K L. Synthesis and Spectroscopy of Lanthanide Ion-doped Y_2O_3 [J]. The Journal of Physical Chemistry B, 2003, 108(1): 136 - 142.

[2] VETRONE F, BOYER J C, CAPOBIANCO J A, et al. Effect of Yb^{3+} Codoping on the Upconversion Emission in Nanocrystalline Y_2O_3: Er^{3+} [J]. The Journal of Physical Chemistry B, 2003, 107(5): 1107 - 1112.

[3] BAI X, SONG H, YU L, et al. Luminescent Properties of Pure Cubic Phase Y_2O_3/Eu^{3+} Nanotubes/Nanowires Prepared by a Hydrothermal Method [J]. The Journal of Physical Chemistry B, 2005, 109(32): 15236 - 15242.

[4] NELSON J A, BRANT E L, WAGNER M J. Nanocrystalline Y_2O_3: Eu Phosphors Prepared by Alkalide Reduction [J]. Chemistry of Materials, 2003, 15(3): 688 - 693.

[5] VETRONE F, BOYER J-C, CAPOBIANCO J A, et al. Concentration-Dependent Near-Infrared to Visible Upconversion in Nanocrystalline and Bulk Y_2O_3: Er^{3+} [J]. Chemistry of Materials, 2003, 15(14): 2737 - 2743.

[6] LI J-G, LI X, SUN X, et al. Monodispersed Colloidal Spheres for Uniform Y_2O_3: Eu^{3+} Red-Phosphor Particles and Greatly Enhanced Luminescence by Simultaneous Gd^{3+} Doping [J]. The Journal of Physical Chemistry C, 2008, 112(31): 11707 - 11716.

[7] KLAASSEN D B M, VAN HAM R A M, VAN RIJN T G M. Energy transfer processes in yttrium oxide activated with europium [J]. Journal of Luminescence, 1989, 43(5): 261-274.

[8] RONDA C R. Phosphors for lamps and displays: an applicational view [J]. Journal of Alloys and Compounds, 1995, 225(1 - 2): 534 - 538.

[9] RONDA C R. Recent achievements in research on phosphors for lamps and displays [J]. Journal of Luminescence,1997,72 - 74(6):49 - 54.

[10] PENG X,MANNA L,YANG W,et al. Shape control of CdSe nanocrystals [J]. Nature,2000,404(6773):59 - 61.

[11] NGUYEN T D,DINH C T,DO T O. Shape- and Size-Controlled Synthesis of Monoclinic ErOOH and Cubic Er_2O_3 from Micro- to Nanostructures and Their Upconversion Luminescence [J]. ACS Nano,2010,4(4):2263 - 2273.

[12] LI G,PENG C,LI C,et al. Shape-Controllable Synthesis and Morphology-Dependent Luminescence Properties of GaOOH: Dy^{3+} and β-Ga_2O_3: Dy^{3+} [J]. Inorganic Chemistry,2010,49(4):1449 - 1457.

[13] QIAN L, ZHU J, CHEN Z, et al. Self-Assembled Heavy Lanthanide Orthovanadate Architecture with Controlled Dimensionality and Morphology [J]. Chemistry-A European Journal,2009,15(5):1233 - 1240.

[14] EL-SAYED M A. Some Interesting Properties of Metals Confined in Time and Nanometer Space of Different Shapes [J]. Accounts of Chemical Research,2001,34(4):257 - 264.

[15] GAO J, GU H, XU B. Multifunctional Magnetic Nanoparticles: Design, Synthesis, and Biomedical Applications [J]. Accounts of Chemical Research,2009,42(8):1097 - 1107.

[16] EKAMBARAM S,MAAZA M. Combustion synthesis and luminescent properties of Eu^{3+}-activated cheap red phosphors [J]. Journal of Alloys and Compounds,2005,395(1 - 2):132 - 134.

[17] KODAIRA C A,STEFANI R,MAIA A S,et al. Optical investigation of nanophosphor prepared by combustion and Pechini methods [J]. Journal of Luminescence,2007,127(2):616 - 622.

[18] PANG Q, SHI J, LIU Y, et al. A novel approach for preparation of Y_2O_3: Eu^{3+} nanoparticles by microemulsion - microwave heating [J]. Materials Science and Engineering: B,2003,103(1):57 - 61.

[19] KONRAD A. Chemical vapor synthesis and luminescence properties of nanocrystalline cubic Y_2O_3: Eu [J]. Journal of Applied Physics,1999,86(6):3129.

[20] ZHANG J,HONG G. Synthesis and photoluminescence of the Y_2O_3: Eu^{3+} phosphor nanowires in AAO template [J]. Journal of Solid State Chemistry,2004,177(4 - 5):1292 - 1296.

[21] SONG S A,JUNG K Y,PARK S B. Preparation of Y_2O_3 Particles by Flame Spray Pyrolysis with Emulsion [J]. Langmuir,2009,25(6):3402 - 3406.

[22] LEE C H,JUNG K Y,CHOI J G,et al. Nano-sized Y_2O_3: Eu phosphor particles prepared by spray pyrolysis [J]. Materials Science and Engineering: B,2005,116(1):59 - 63.

[23] HSU W P,RONNQUIST L,MATIJEVIC E. Preparation and properties of monodispersed colloidal particles of lanthanide compounds. 2. Cerium(IV) [J]. Langmuir,1988,4(1):31 - 37.

[24] AIKEN B A R,HSU W P,MATIJEVI Ć E. Preparation and Properties of Monodispersed Colloidal Particles of Lanthanide Compounds: III,Yttrium(III) and Mixed Yttrium(III)/Cerium(III) Systems [J]. Journal of the American Ceramic Society,1988,71(10):845 - 853.

[25] WANG H,LIN C K,LIU X M,et al. Monodisperse spherical core-shell-structured phosphors obtained by functionalization of silica spheres with Y_2O_3: Eu^{3+} layers for field emission displays [J]. Applied Physics Letters,2005,87(18):181907.

[26] YAVUZ M S,CHENG Y,CHEN J,et al. Gold nanocages covered by smart polymers for controlled release with near-infrared light [J]. Nat Mater,2009,8(12):935 - 939.

[27] HYUK IM S,JEONG U,XIA Y. Polymer hollow particles with controllable holes in their surfaces [J]. Nat Mater,2005,4(9):671 - 675.

[28] JIA G,YANG M,SONG Y,et al. General and Facile Method To Prepare Uniform Y_2O_3: Eu Hollow Microspheres [J]. Crystal Growth & Design,2008,9(1):301 - 307.

[29] ZHANG N, LIU X, YI R, et al. Selective and Controlled Synthesis of Single-Crystalline Yttrium Hydroxide/Oxide Nanosheets and Nanotubes [J]. The Journal of Physical Chemistry C,2008,112(46):17788 - 17795.

[30] MAO Y,HUANG J Y,OSTROUMOV R,et al. Synthesis and Luminescence Properties of Erbium-Doped Y_2O_3 Nanotubes [J]. The Journal of Physical Chemistry C,2008,112(7):2278 - 2285.

[31] ZHANG N,BU W,XU Y,et al. Self-Assembled Flowerlike Europium-Doped Lanthanide Molybdate Microarchitectures and Their Photoluminescence Properties [J]. The Journal of Physical Chemistry C,2007,111(13):5014 - 5019.

[32] XU Z,LI C,LI G,et al. Self-Assembled 3D Urchin-Like $NaY(MoO_4)_2:Eu^{3+}/Tb^{3+}$ Microarchitectures: Hydrothermal Synthesis and Tunable Emission Colors [J]. The Journal of Physical Chemistry C,2010,114(6):2573 - 2582.

[33] YANG J,LI C,QUAN Z,et al. Self-Assembled 3D Flowerlike Lu_2O_3 and $Lu_2O_3:Ln^{3+}$ (Ln = Eu,Tb,Dy,Pr,Sm,Er,Ho,Tm) Microarchitectures: Ethylene Glycol-Mediated Hydrothermal Synthesis and Luminescent Properties [J]. The Journal of Physical Chemistry C,2008,112(33):12777 - 12785.

[34] SOUNART T L,LIU J,VOIGT J A,et al. Sequential Nucleation and Growth of Complex Nanostructured Films [J]. Advanced Functional Materials,2006,16(3):335 - 344.

[35] LIU J,LV H,WANG Z,et al. Correlations Between Shape and Near Infrared Reflective Properties of Nano/Micro-Yttria [J]. Journal of Nanoscience and Nanotechnology,2011,11(4):3616 - 3620.

[36] YANG P,GAI S,LIU Y,et al. Uniform Hollow $Lu_2O_3:Ln$ ($Ln = Eu^{3+},Tb^{3+}$) Spheres: Facile Synthesis and Luminescent Properties [J]. Inorganic Chemistry,2011,50(6):2182 - 2190.

[37] JIA G,YOU H,SONG Y,et al. Facile Synthesis and Luminescence of Uniform Y_2O_3 Hollow Spheres by a Sacrificial Template Route [J]. Inorganic Chemistry,2010,49(17):7721 - 7725.

[38] ZHANG L,JIA G,YOU H,et al. Sacrificial Template Method for Fabrication of Submicrometer-Sized $YPO_4:Eu^{3+}$ Hierarchical Hollow Spheres [J]. Inorganic Chemistry,2010,49(7):3305 - 3309.

由纳米管自组装成花状,管状,球状 $Y_2O_3:Eu^{3+}$ 的可控合成

邹　兴, 刘浦俊, 余锡宾*

(上海师范大学 生命与环境科学学院,上海 200234)

摘　要: 在没有任何模板剂的条件下,通过水热法将 $Y(OH)CO_3$ 纳米片自组装卷曲并经后期退火得到单分散的花状 Y_2O_3. 通过调节 $Y(CH_3COO)_3$ 的浓度,我们得到了长约 150 nm、直径 40 nm 左右且分散均匀的 Y_2O_3 纳米管及粒径在 30 nm 左右的单分散 Y_2O_3 纳米球. Eu^{3+} 引入并没有影响其形貌. 在紫外光的激发下,花状及球状的 $Y_2O_3:0.05Eu^{3+}$ 样品均显示强的红光发射,对应于 Eu^{3+} 的特征峰.

关键词: $Y_2O_3:Eu^{3+}$; 自组装; 发光性能

(责任编辑: 郁　慧)